ADVANCED SUSTAINABLE SYSTEMS
www.advsustainsys.com

Fabrication of Superinsulating Poly(Urethane-Isocyanurate) Aerogels Derived from Upcycled Polycarbonate

*Ivona Glišić, Keita Saito, Chang-lin Wang, Christos Pantazidis, Fabian Eisenreich, and Željko Tomović**

Upcycling plastic waste into advanced functional materials is a sustainable approach to mitigate plastic accumulation and its associated environmental hazards. In this work, bisphenol-A polycarbonate (BPA-PC) is upcycled into an aromatic Mannich polyol (MP) via a simple one-pot process combining organocatalyzed methanolysis followed by a Mannich reaction. MP further serves as a precursor for poly(urethane-isocyanurate) (PUR-PIR) aerogels. The resulting PUR-PIR aerogels are prepared with different isocyanate indices and demonstrate low bulk densities (<195 mg cm^{-3}), and high specific surface areas (≈ 200 m^2 g^{-1}), along with outstanding mechanical performance, and ultralow thermal conductivity (≈ 17 mW m^{-1} K^{-1}). Importantly, PUR-PIR aerogels prepared from pristine or waste BPA-PC exhibit comparable material performance. This work highlights the potential of upcycling plastic waste into superinsulating aerogels with tunable material properties.

1. Introduction

The rapid increase in production and usage of plastics overhauled our lives in the last decades.[1] Even though plastics have an impactful role to society due to their versatility and convenience, the poor management of plastic waste endangers ecosystems and environment.[2] Rather than relying on the established inefficient and traditional linear model (take-make-waste), a circular economy model offers a more sustainable alternative by emphasizing resource regeneration, waste valorization, and continuous recycling.[3,4] Among the various strategies, upcycling stands out as a method that turns waste into valuable resources, which can be used to prepare advanced materials with a renewed purpose.[5–7] Within the spectrum of plastic waste streams, bisphenol-A polycarbonate (BPA-PC) emerges as a particularly promising target for valorization, as most post-consumer BPA-PC ends up in landfills, where it potentially leaches BPA—a compound linked to significant environmental and health hazards.[8]

BPA-PC is a thermoplastic polymer with excellent mechanical performance and high glass transition temperature (T_g ≈ 150 °C).[9] Such properties render polycarbonates as highly suitable for various applications across the electronics, automotive, and architectural industries.[10] Mechanical recycling methods, such as grinding and re-extrusion can be employed; however, this typically results in diminished polymer quality, limiting the potential for extended and repeated reusability.[11] Therefore, more effective strategies are needed to manage BPA-PC waste. One promising approach to effectively treat BPA-PC waste is selective chemical depolymerization, which can be achieved through hydrolysis, alcoholysis, or aminolysis.[12–15] Such methods permit the controlled recovery of BPA and organic carbonates. These recovered building blocks, or their derivatives, have been used, in some cases, as precursors for preparing value-added advanced polymers such as poly(carbonate-imine)s,[16] poly(aryl ether sulfone)s[17] and industrially relevant—poly(urethane)s (PUR)s.[18]

The importance of PURs lies in their structural tunability and performance versatility, which make them excellent candidates for applications such as coatings, adhesives, and foams.[19,20] While foams contain larger pore sizes (≈ 100–250 µm), PUR aerogels possess much smaller pore sizes (≈ 2–50 nm), which restrict gas molecule collisions and minimize heat transfer via gaseous conduction, known as the Knudsen effect.[21–23] As a result, PUR aerogels exhibit superior thermal insulation with thermal conductivities that can reach values below 0.020 W m^{-1} K^{-1}. In addition to their insulation ability, their high porosity (> 80%) and large specific surface area (>100 m^2 g^{-1}) make PUR aerogels ideal for applications in energy storage, batteries, and separation technologies.[24,25]

Despite their low thermal conductivity, PUR aerogels are often inferior in terms of mechanical and thermal stability. Therefore, to extend their applicability, various molecular design strategies have been employed to enhance their properties.[20] For

I. Glišić, K. Saito, C.-l. Wang, C. Pantazidis, F. Eisenreich, Ž Tomović
Polymer Performance Materials Group
Department of Chemical Engineering and Chemistry and Institute for Complex Molecular Systems (ICMS)
Eindhoven University of Technology
Eindhoven 5600 MB, The Netherlands
E-mail: z.tomovic@tue.nl

The ORCID identification number(s) for the author(s) of this article can be found under https://doi.org/10.1002/adsu.202500525

DOI: 10.1002/adsu.202500525

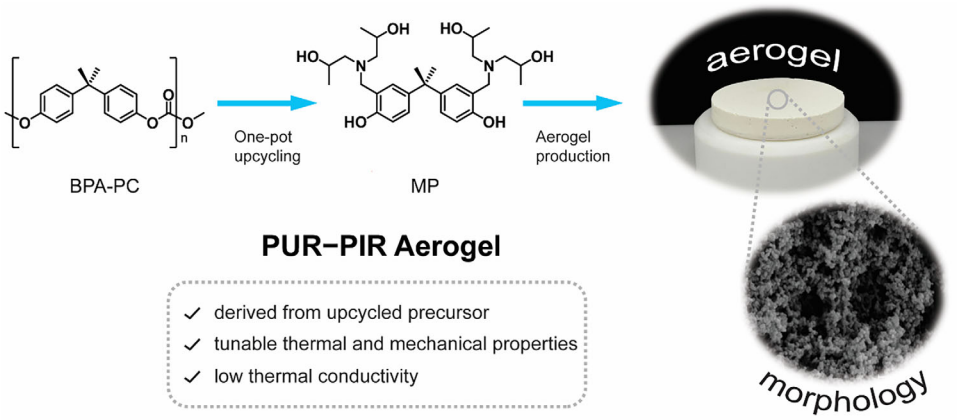

Figure 1. Schematic of the upcycling of BPA-PC into high-performance PUR-PIR aerogels.

instance, the incorporation of aromatic polyols improves the crosslink density and mechanical strength of PUR materials.[26] Another effective strategy involves the integration of isocyanurate (PIR) moieties to form PUR-PIR networks, which further enhance thermal stability and structural robustness.[27] The first attempt to create PUR-PIR aerogels was made in the 1990s by Biesmans et al.[28] Since then, significant advancements have been made, ranging from fundamental studies on the roles of catalysts[29] and solvents[30] to application-driven innovations, such as shape-memory and superelasticity.[31,32] Despite these advancements, the use of upcycled polymer waste for the preparation of high-performance PUR-PIR aerogels remains unexplored.

In our pursuit of sustainable materials innovation, we bridge this gap by upcycling BPA-PC waste into high-performance PUR-PIR aerogels with excellent thermal and mechanical properties (**Figure 1**). To achieve this, we developed a protocol to convert BPA-PC into a Mannich polyol (MP) via a facile one-pot reaction, minimizing purification steps and waste generation.[19,33–36] This process involves an organocatalyzed methanolysis reaction to yield BPA,[33] which is subsequently reacted in the same vessel with oxazolidine through a Mannich reaction to produce MP.[34–36] The resulting Mannich polyol, containing an aromatic moiety, high hydroxyl functionality, and catalytic tertiary amines, serves as a monomer that both accelerates hydroxyl–isocyanate reactions and forms a crosslinked network upon reaction with an aromatic multifunctional isocyanate, enabling the efficient synthesis of PUR-PIR aerogels. These PUR-PIR aerogels significantly outperform conventional PUR-PIR foams, exhibiting exceptional thermal insulation with values as low as 16.6 mW m^{-1} K^{-1}.[21] Furthermore, their high aromatic content imparts excellent mechanical performance, with no signs of collapse or cracking, thereby positioning them as high-performance aerogels. Overall, our findings demonstrate that upcycling of (pristine or postconsumer) BPA-PC into functional monomers enables the reproducible production of advanced aerogels that meet rigorous technical requirements.

2. Results and Discussion

2.1. Synthesis of Mannich Polyol (MP)

To achieve efficient upcycling of BPA-PC, we developed a one-pot method for synthesizing MP by integrating depolymerization of (pristine or postconsumer) BPA-PC with a subsequent Mannich reaction (**Figure 2a**). In the first phase of the reaction, BPA-PC was depolymerized via methanolysis using 4 molar equivalents of methanol and 1,5,7-triazabicyclo[4.4.0]dec-5-ene (TBD) as a basic organocatalyst in toluene at 60 °C for 6 h. Complete consumption and depolymerization of the BPA-PC pellets were confirmed by ^{1}H NMR spectroscopy analysis of the reaction mixture. The ^{1}H NMR spectrum shows the quantitative formation of BPA and dimethyl carbonate (DMC) with no other formed byproducts (Figure S1, Supporting Information). DMC and methanol were removed via distillation at 100 °C, while BPA, TBD, and toluene remained in the reaction vessel. In the second phase, the Mannich reaction was carried out with the addition of oxazolidine and increasing the temperature to 90 °C for 6 h. Since BPA offers four reactive *ortho* positions susceptible to reaction with oxazolidine, it serves as an ideal scaffold for constructing multifunctional polyols. To achieve di-substitution on each aromatic ring, a 1:2 molar ratio of BPA to oxazolidine was used, resulting in the formation of MP with four secondary hydroxyl groups. After the completion, the reaction mixture was treated with an ion exchange resin to remove the TBD catalyst, followed by the removal of toluene under reduced pressure yielding MP with 84% yield. The resulting MP was characterized by ^{1}H NMR spectroscopy, which revealed characteristic chemical shifts corresponding to methylene linkages at 3.7 ppm (Figure 2b).

2.2. Fabrication of PUR-PIR Aerogels

To synthesize PUR-PIR aerogels, we employed commercially available Lupranate M20S isocyanate (M20S) and MP (**Figure 3**). M20S is a mixture of oligomeric methylene diphenyl polyisocyanates with an average isocyanate functionality of 2.7, which is

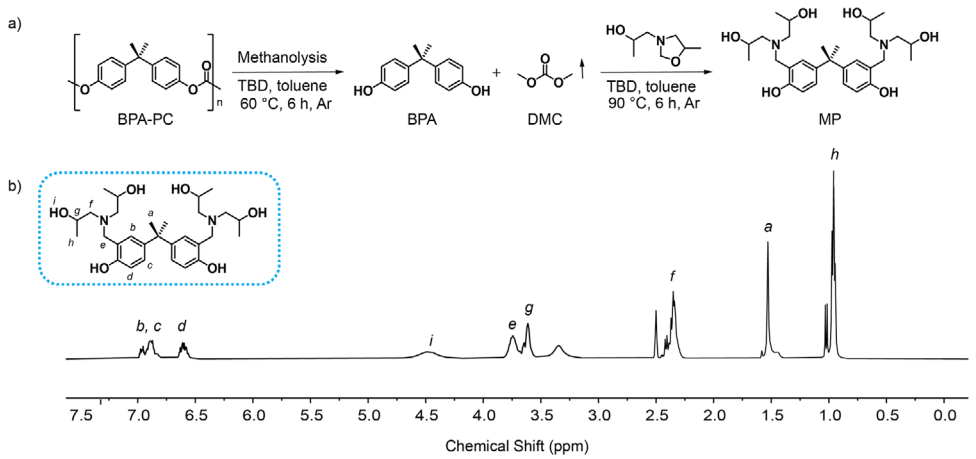

Figure 2. a). One-pot synthesis of MP, b) ^{1}H NMR spectrum of MP (DMSO-d_6, 400 MHz, 20 °C).

highly reactive toward hydroxyl groups. Additionally, M20S was chosen for its high aromatic content to enhance the stability of the formed networks. While MP contains six hydroxyl groups, the four secondary hydroxyl groups are found to be significantly more reactive toward urethane formation compared to the other two phenolic hydroxyl groups.[19] Hence, the number of reactive hydroxyl groups of MP is considered to be four. A beneficial side effect of MP's chemical structure is that the tertiary amines within the molecule catalyze the desired urethane formation, thereby further enhancing the crosslinking reaction. In addition, the thermal stability of the polymer network is a key factor for the development of high-performance materials. In PUR aerogels, incorporating PIR structures is an effective strategy, as PIR—formed through the trimerization of isocyanate units—is renowned for its exceptional thermal resistance. To initiate PIR formation alongside the PUR reaction, we employed the commercially available and industrially relevant trimerization catalyst Dabco K-15 (75% potassium 2-ethyl hexanoate, 25% diethylene glycol).[37]

The PUR-PIR aerogel fabrication route consists of multiple steps: mixing dissolved precursors, polyaddition reaction resulting in gelation followed by aging, solvent exchange, and finally supercritical-CO_2 drying (SCD) (Figure 3). To investigate the aerogel performance with varying PUR and PIR content, three different formulations with different isocyanate-to-hydroxyl ratios were tested. The isocyanate index, defined as ([isocyanate]/[MP secondary hydroxyl]*100), was set as 125, 150, and 175, respectively, while the initial concentration of the precursors

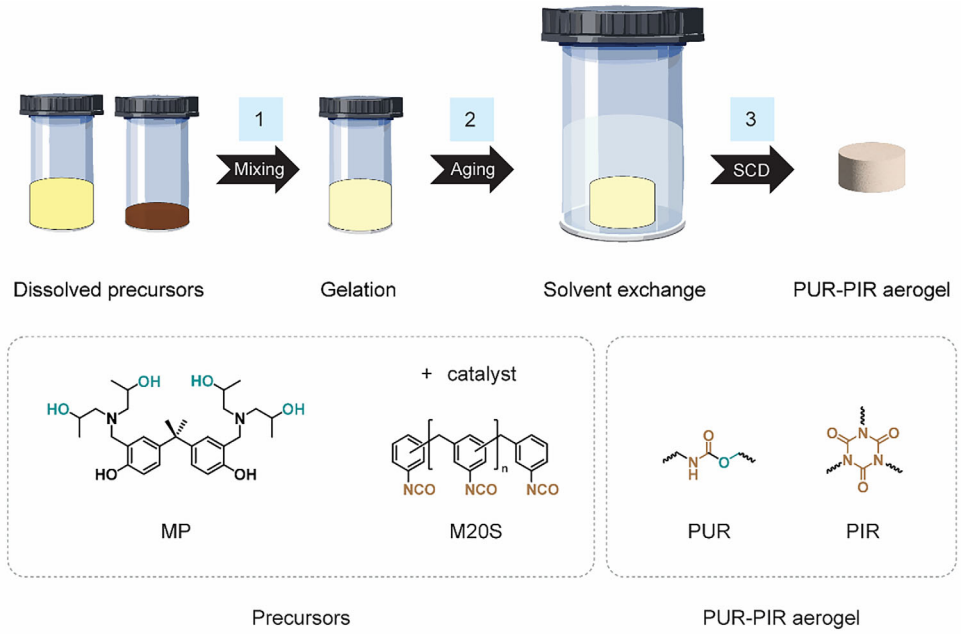

Figure 3. Fabrication of PUR–PIR aerogels: (1) mixing dissolved precursors in DEK followed by gelation, (2) aging of organogels followed by solvent exchange, and (3) SCD to obtain PUR-PIR aerogel.

Table 1. Physical properties of PUR-PIR aerogels.

Aerogel	Isocyanate index[a)]	Linear shrinkage [%][b)]	Bulk density [mg cm^{-3}]	Skeletal density [g cm^{-3}][c)]	Porosity [%][d)]	Specific surface area [m^2 g^{-1}][e)]	Mesopore volume [cm^3 g^{-1}][f)]	Average particle size [nm][g)]
PUR-PIR 125	125	11	162	1.23	87	93	0.31	43 ± 8
PUR-PIR 150	150	14	184	1.24	85	118	0.45	42 ± 8
PUR-PIR 175	175	17	195	1.26	84	201	0.62	40 ± 7

[a)] Isocyanate index = [isocyanate]/[MP secondary hydroxyl]*100; [b)] Considered as a diameter change; [c)] Measured using helium pycnometer (Experimental Section); [d)] Porosity was calculated using the bulk and skeletal density (Experimental Section); [e)] BET method was used to extrapolate the specific surface area; [f)] BJH method was used to determine the mesopore volume from desorption isotherms; [g)] Determined using ImageJ software from a data set of 50 particles.

in diethyl ketone (DEK) was kept at 0.12 g cm^{-3}. Following the aerogel fabrication route, three different PUR-PIR aerogels were prepared and abbreviated as PUR-PIR 125, PUR-PIR 150, and PUR-PIR 175 (Experimental Section, Table S1 in Supporting Information).

It was found that full isocyanate conversion to its derivatives, including urethane and isocyanurate, cannot be achieved at room temperature (Figure S2, Supporting Information). To facilitate the reaction, the reaction temperature was raised to 50 °C during the initial gelation stage. After 2 to 5 min, stable opaque organogels were obtained, which were then aged for 2 h at 50 °C, followed by 48 h at room temperature to ensure complete conversion of the precursors and reinforce the integrity of the resulting network. The success of the reaction was confirmed with Fourier-transform infrared (FT-IR) spectroscopy, where no unreacted isocyanate could be observed (Figure S3, Supporting Information). All organogels exhibited no shrinkage after the aging step. Finally, to remove the pore-filling DEK, organogels were dried using SCD, resulting in three stable PUR-PIR aerogels.

2.3. Physical Properties of PUR-PIR Aerogels

The synthesized PUR-PIR aerogels were thoroughly characterized to assess their physical properties, which are summarized in **Table 1**. First, linear shrinkage and bulk density were measured and calculated. The observed values of linear shrinkage (11–17%) are typical for PUR-PIR aerogels reported so far.[28,38] When increasing the isocyanate index, PUR-PIRs exhibited greater linear shrinkage (≈ 17%), which occurred during the SCD step. Furthermore, the bulk densities of the aerogels echoed the trend in linear shrinkage ranging from 162 to 195 mg cm^{-3}, where the lowest bulk densities were attributed to PUR-PIR aerogels with lower isocyanate index.

Morphological and structural analysis of PUR-PIR aerogels was performed using helium pycnometer, nitrogen physisorption, and scanning electron microscopy (SEM), to obtain skeletal densities, specific surface areas, pore volume distributions, and SEM micrographs (**Figure 4**). Overall, the prepared PUR-PIR aerogels exhibited complex interconnected structures with mesoporous domains characteristic for aerogels. Their high porosity (84–87%), as an essential property of lightweight materials, was calculated from the bulk and skeletal density (1.23–1.26 g cm^{-3}) values. Notably, PUR-PIR aerogels with higher isocyanate indices exhibited lower porosities, consistent with their higher bulk densities. The pore structures of PUR-PIR aerogels were further analyzed using nitrogen physisorption experiments. The nitrogen adsorption-desorption experiments showed type IV isotherms typically associated with mesoporous materials (Figure 4b). Furthermore, the BET (Brunauer-Emmet-Teller) method was used to extrapolate the specific surface area of PUR-PIR aerogels, ranging from ≈ 100 to 200 m^2 g^{-1}. Importantly, the increase in isocyanate index also results in higher values of specific surface area. Additionally, a similar trend applies for the accessible mesopore volumes of PUR-PIR aerogels that range from 0.31 to 0.62 cm^3 g^{-1}. Furthermore, SEM analyses were performed, which revealed that all PUR-PIR aerogels exhibit isotropic particle-like structures with homogenous pore structures and no visible defects (Figure 4a; Figure S4, Supporting Information). The particle sizes within the aerogel network were measured to range from 20 to 60 nm using ImageJ software (Figure S5, Supporting Information). Additionally, histograms of 50 individual particle sizes showed a tendency for PUR-PIR aerogels with higher isocyanate index to shift toward smaller particle sizes. This behavior is likely attributed to the distinct chemical composition of the aerogels, as PUR and PIR exhibit different solubilities in DEK. These differences influence phase separation behavior[39] resulting in distinct particle formation and variations in surface morphology.

For long-term applications, it is crucial to test the aerogel stability in very humid conditions since water sorption can significantly increase their thermal conductivities.[40] To assess this, we performed dynamic vapor sorption experiments for PUR-PIR aerogels (90% relative humidity, 12 h, 25 °C). All PUR-PIR aerogels reached sorption saturation level during 2 h of exposure, after which no further change in mass was observed (< 8%, Figure S6, Supporting Information). The synergetic effect of both the chemistry and morphology of PUR-PIR aerogels likely affects the water sorption in moist environments. Importantly, the amount of water sorbed was low proving that PUR-PIRs are suitable candidates for various applications, even in extremely humid environments.

2.4. Thermal and Mechanical Properties of PUR-PIR Aerogels

As a result of their intricate structure and high mesoporosity, aerogels are considered as excellent thermal insulation materials. The key to their exceptional insulation lies in minimizing heat transfer through both the solid and the gas phases, with only a minor contribution of the radiation effect.[40] Specifically, as mesoporous materials, aerogels display reduced heat transfer through the gas phase, due to the Knudsen effect, where the gas molecule collisions are minimized, leading to low gaseous heat conduction. Additionally, morphology and bulk density of aerogels significantly influence the heat transfer through the solid phase.[40,41] The thermal conductivity of PUR-PIR aerogels

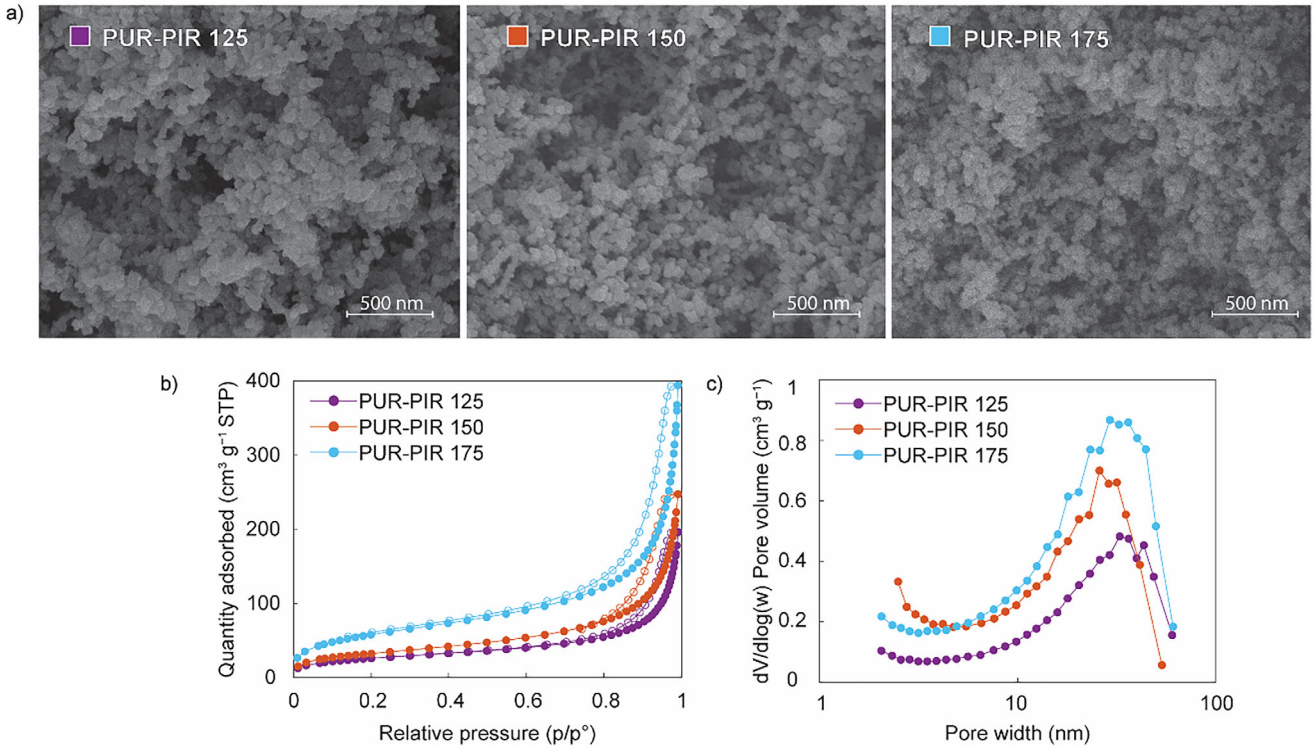

Figure 4. Structural characterization. a) SEM micrographs, b) BET isotherms, and c) pore size distribution (BJH) of PUR-PIR aerogels.

was measured using a heat flow meter (HFM, **Table 2**, **Figure 5a**). PUR-PIR 125, with the lowest specific surface area and mesopore volume, exhibited the highest thermal conductivity of 21.7 mW m^{-1} K^{-1}. In contrast, increasing the isocyanate index led to improved insulation performance: PUR-PIR 150 and PUR-PIR 175 exhibited lower thermal conductivities of 18.4 and 16.6 mW m^{-1} K^{-1}, respectively—surpassing several conventional insulation materials and other aerogels (Figure S7, Supporting Information).[42] Previous systematic studies on PUR-PIR aerogels indicate that differences in heat transfer through the gas phase have a greater impact on effective thermal conductivity compared to heat transfer through the solid phase, which is consistent with our findings.[41] These results demonstrate that the effective thermal conductivity of PUR aerogels can be reduced with increasing isocyanate index, likely due to an increase in specific surface area and mesopore volume.

Table 2. Thermal properties of PUR-PIR aerogels.

Aerogel	Thermal conductivity [mW m^{-1} K^{-1}][a)]	$T_{d5\%}$ [°C][b)]	R_{595} [%][c)]
PUR-PIR 125	21.7	215	14
PUR-PIR 150	18.4	222	14
PUR-PIR 175	16.6	227	21

[a)] Thermal conductivity of samples (size: 50 mm diameterand 10 mm thickness) was measured with a heat flow meter (Thermtest Inc., HFM-25), at 23 °C and relative humidity 35%; [b)] Temperature at which 5% weight loss occurred acquired through TGA; [c)] Char formation yield at 595 °C acquired through TGA.

Additionally, the thermal stability of PUR-PIR aerogels is crucial for their applicability. The thermal resistance of PUR-PIR aerogels was evaluated using thermogravimetric analysis (TGA, Figure 5b). PUR-PIR aerogels exhibited multi-step degradation curves, with $T_{d5\%}$ values between 215 and 227 °C, which are typical for urethane-based materials.[19] The first degradation step at 220 °C corresponds to a simple cleavage of urethane bonds, while PIR cleavage occurs at higher temperatures around 400 °C. In addition, the high aromatic content of PUR-PIR aerogels promotes char formation, resulting in residual mass of 14–21%. PUR-PIR aerogels high thermal stability coupled with exceptionally low thermal conductivity further enhances their potential for applications as thermal insulation materials.

Next to their excellent thermal properties, high-performance aerogels are required to be stable and retain their shape and porous features upon handling. The high aromaticity of MP and M20S, along with possible π-π stacking within the aromatic structures, was strategically implemented into the material design to enhance the mechanical robustness and resilience of PUR-PIR aerogels. Uniaxial compression tests revealed nonlinear stress-deformation behavior, with all aerogels maintaining structural integrity even at 68–75% deformation without any cracks (Figure 5c). Notably, all PUR-PIRs required high compressive strength for 15% deformation ranging from 143 to 267 kPa (Table S4, Figure S8, Supporting Information). Among them, PUR-PIR 175 exhibited the highest compressive strength, likely due to its increased crosslink density.[27] In general, all PUR-PIR aerogels showed exceptional mechanical stability under high compressive stresses, confirming their durability and resilience.

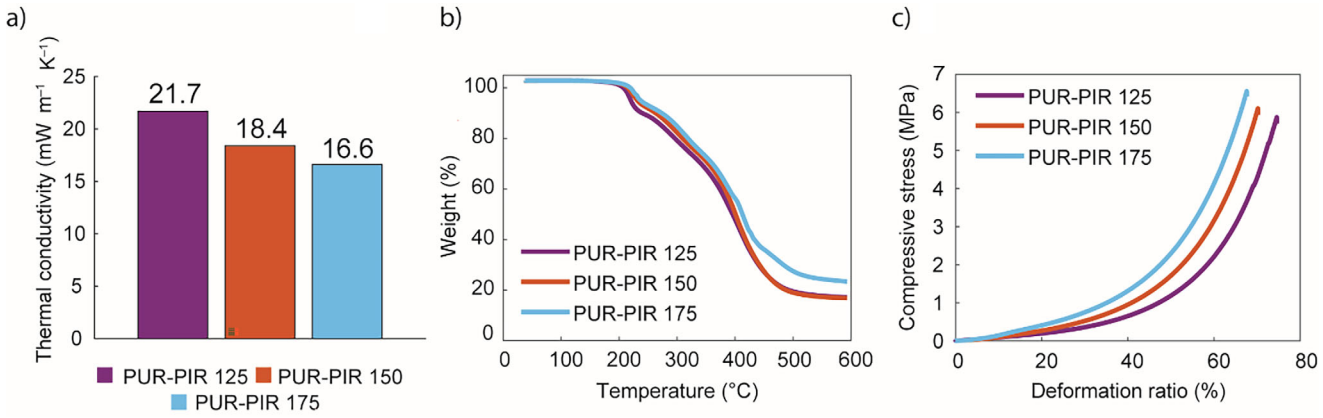

Figure 5. Thermal and mechanical characterization. a) Thermal conductivity, b) thermal degradation curves, and c) uniaxial compression curves of PUR-PIR aerogels.

2.5. Fabrication of PUR-PIR Aerogels From Postconsumer BPA-PC Waste

To demonstrate that PUR-PIR aerogels can be synthesized from postconsumer BPA-PC, we applied our established upcycling strategy, however, in this case, by utilizing discarded safety goggles as the raw material (**Figure 6a**). First, MP derived from postconsumer BPA-PC (MP-W) was successfully synthesized with 86% yield (Experimental section, Figures S9,S10, Supporting Information), showing the same purity as the original MP (obtained

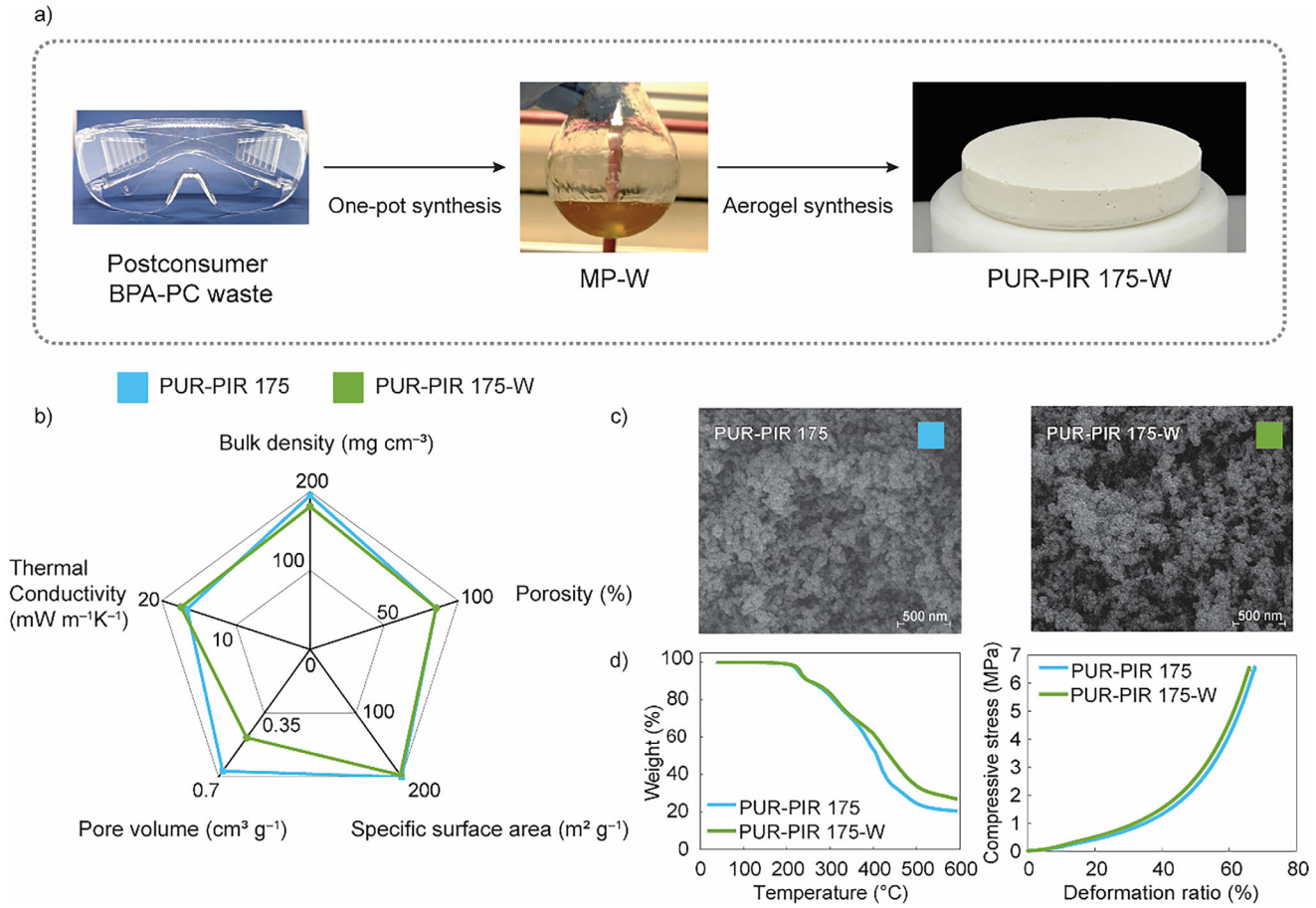

Figure 6. a) Fabrication of PUR-PIR 175-W obtained from postconsumer BPA-PC, b) radial graph comparing physical properties of PUR-PIR 175 and PUR-PIR 175-W, c) SEM micrographs, and d) thermal degradation (bottom left) and uniaxial compression (bottom right) measurements of PUR-PIR 175 and PUR-PIR 175-W.

Table 3. Thermal properties of PUR-PIR 175 and PUR-PIR 175-W.

Aerogel	Thermal conductivity [mW m^{-1} K^{-1}][a)]	$T_{d5\%}$ [°C][b)]	R_{595} [%][c)]
PUR-PIR 175	16.6	227	21
PUR-PIR 175-W	17.4	230	27

[a)] Thermal conductivity of samples (size: 50 mm diameterand 10 mm thickness) was measured with a heat flow meter (Thermtest Inc., HFM-25), at 23 °C and relative humidity 35%. [b)] Temperature at which 5% weight loss occurred acquired through TGA. [c)] Char formation yield at 595 °C acquired through TGA.

from pristine BPA-PC). Second, an aerogel with an isocyanate index of 175 (PUR-PIR 175-W) was prepared from MP-W. PUR-PIR 175-W exhibited nearly identical physical and material properties, which were assessed and compared to the pristine PUR-PIR 175 (**Table 3**, Figure 6). SEM and BET analysis of PUR-PIR 175-W confirmed particle-like morphology and mesoporous domains, which were further quantified with average particle size (41±8 nm), specific surface area (≈ 198 m^2 g^{-1}), and pore volume (≈ 0.45 cm^3 g^{-1}). Regardless of the BPA-PC source, the physical properties of PUR-PIR aerogels remained within a consistent and reproducible range (Figure 6b; Figure S11, Supporting Information). PUR-PIR 175-W preserved excellent thermal and mechanical properties as well. Most importantly, the thermal conductivity of PUR-PIR 175-W was nearly identical to pristine PUR-PIR 175 with a value of 17.4 mW m^{-1} K^{-1}. TGA demonstrated similar multi-step degradation profiles, with minor differences in onset degradation temperature and char residue at 595 °C. Slight differences observed around 400 °C may suggest minor variation in PIR content within the aerogel structure. Last, uniaxial compression test indicated almost identical mechanical strength, and non-linear trend in stress-strain profiles of PUR-PIR 175 and PUR-PIR 175-W. To conclude, PUR-PIR aerogels obtained from postconsumer BPA-PC retain outstanding material performance and exhibit ultralow effective thermal conductivity.

3. Conclusion

In conclusion, this study presents an effective strategy for upcycling BPA-PC into high-performance PUR-PIR aerogels. First, we successfully upcycled BPA-PC into MP through a facile one-pot process involving methanolysis followed by a Mannich reaction, yielding a monomer of high purity with an isolated yield of 84%. Second, MP was then used to synthesize PUR-PIR aerogels with varying isocyanate indices. The aerogels exhibited low bulk densities (< 195 mg cm^{-3}), high porosities (> 84%), ultralow thermal conductivities (16.6–21.7 mW m^{-1}K^{-1}), and excellent mechanical properties. More importantly, efficient reproducibility of these PUR-PIR aerogels was successfully demonstrated using postconsumer BPA-PC waste. The PUR-PIR aerogel from waste showed nearly identical properties to the PUR-PIR aerogel obtained from pristine BPA-PC. To conclude, our PUR-PIR aerogels, obtained using an upcycling strategy, offer a set of tunable material properties and show great potential for various thermal insulation applications. By incorporating waste valorization, our approach offers a practical solution toward more sustainable high-performance aerogels.

4. Experimental Section

Materials: BPA-PC (M_w ≈ 45,000 g mol^{-1}), anhydrous methanol, TBD, paraformaldehyde, Amberlyst 15 hydrogen form and DEK were purchased from Merck. DMSO-d_6, (99.9%) was purchased from Cambridge Isotope Laboratories. Toluene was purchased from Biosolve and stored over 4Å molecular sieves. Oligomeric methylene diphenyl polyisocyanate (Lupranate M20S, average functionality 2.7) and Dabco K-15 (75% potassium 2-ethyl hexanoate dissolved in diethylene glycol) were provided by BASF Polyurethanes GmbH. Liquid CO_2 (grade 2.7), N_2 (grade 5.0), and He (grade 4.6) were purchased from Linde Gas B.V.

Synthesis of Mannich Polyol: Prior the polyol synthesis, oxazolidine was synthesized as reported in supplementary information (Scheme S1, Figure S12, Supporting Information). The synthesis of MP was performed in a 3-necked-round-bottom flask equipped with a magnetic stirrer and reflux condenser. A mixture of BPA-PC (60 g, 236.2 mmol, 1 eq.), methanol (30.3 g, 944.9 mmol, 4 eq.), TBD (0.9 g, 7.1 mmol, 0.03 eq.) was first purged under Ar flow for 15 min before heating the mixture to 60 °C for 6 h. Full depolymerization to BPA and DMC was confirmed by ^{1}H NMR spectroscopy (Figure S1, Supporting Information). DMC and methanol were subsequently removed by distillation at 100 °C, while TBD, BPA and toluene remained in the flask. Next, oxazolidine (68.6 g, 472.4 mmol, 2 eq.) was added to the flask and the reaction temperature was set to 90 °C. Upon completion, TBD catalyst was removed using acidic ion exchange resin (Amberlyst 15), followed by toluene removal under reduced pressure. MP was obtained in high yield (51.3 g, 84%). The same protocol was used for the synthesis of MP-W, derived from discarded BPA-PC safety goggles (Figures S9 and S10, Supporting Information, yield: 86%).

Fabrication of PUR-PIR Aerogels: PUR-PIR aerogels were prepared by mixing component A (M20S) and component B (MP) in presence of a catalyst (Dabco K-15) at 50 °C. The isocyanate index was maintained at 125, 150, and 175, while the amount of Dabco K-15 was kept constant (1.25 wt.%) as well as precursor concentration (0.12 g cm^{-3}). The detailed composition of all samples is provided in Supporting Information (Table S1, Supporting Information).

To illustrate the fabrication process, it was further elaborated on the PUR-PIR 175 synthesis: M20S (2.56 g, 19.17 mmol) was dissolved in 7 g of DEK and MP (1.42 g, 10.95 mmol) and Dabco K-15 (50 mg, 1.25 wt.%) were dissolved in 20 g of DEK. Gelation was initiated by combining both solutions into one vial, which was vigorously shaken (≈ 10 s) and poured into a PTFE mold with an inner diameter 61 mm, at 50 °C. After gelation, aging was performed at 50 °C for 2 h and then at room temperature for 48 h, in a tightly sealed PTFE mold to prevent any DEK evaporation. The organogels were washed four times with DEK (4 × 300 mL x 24 h) and then transferred to an SCD autoclave, fully submerged in DEK, and quickly sealed. Drying was performed in four cycles, maintaining the pressure at 120 bar and temperature above 60 °C. The resulting aerogels were then stored in a vacuum oven at 80 °C for 12 h remove any residual solvent traces and were after stored in a desiccator chamber (relative humidity 35%). The standard aerogel sample size was ≈ 50 mm in diameter and 10 mm in thickness. Smaller samples, with dimensions of ≈ 23 mm in diameter and 16 mm in thickness, were prepared specifically for compression testing.

Chemical Characterization: The chemical structures relevant for the synthesis of MP, were identified by nuclear magnetic resonance (NMR) spectroscopy, performed on a Bruker UltraShield spectrometer (400 MHz for ^{1}H NMR) at 20 °C using DMSO-d_6 as the solvent.

FT-IR analysis was conducted using a Thermo Fisher Scientific Nicolet iS20 spectrometer equipped with an Attenuated Total Reflection (ATR) accessory. Spectral data were collected over the range of 4000–450 cm^{-1}.

Physical Characterization: Bulk density (ρ_b) was calculated as a ratio of measured aerogel mass and geometric volume, which was measured with

a calliper. Skeletal density (ρ_s) was measured using helium pyconometer (AccyPyc II 1345, helium grade 4.6) where 10 data points were obtained from 10 equilibrium cycles. Porosity (Π) was calculated using Equation (1), where ρ_b and ρ_s are bulk and skeletal density:

$$\Pi = 100\% * \left(1 - \frac{\rho_b}{\rho_s}\right) \quad (1)$$

To assess their stability in moist environments, dynamic vapor sorption (DVS) measurements were measured using DVS Resolution Dual Vapor Gravimetric Sorption Analyzer 1. All samples (≈ 10 mg) were first exposed to 0% relative humidity (RH) for 2 h and then to 90% RH (25 °C) for 12 h. Samples' change in mass was detected and attributed to the amount of water sorbed.

Structural Characterization: Scanning electron microscopy (SEM, FEI Quanta 200 3D) was used to characterize aerogel morphology at an acceleration voltage 15 kV. Before testing, samples were sputtered with gold (40 mA, 40 s). Specific surface area and pore size distribution were measured using Braunauer-Emmett-Teller (BET) and Barrett-Joyer-Halenda (BJH) models respectively (Tristar II Plus, N_2 grade 5.0, He grade 4.7). Prior to the measurement, the samples were outgassed at 80 °C for 2 h.

Testing Thermal and Mechanical Properties: Thermogravimetric analysis (TGA) was performed to measure thermal degradation profiles of aerogels ($T_{d5\%}$, R_{595}). The measurements were performed using TGA 550 (TA Instruments) under N_2 atmosphere at a constant heating rate 10 °C min^{-1} from 40 to 600 °C, where the sample size was ≈ 5 mg. The thermal conductivity was measured by a heat flow meter (Thermtest Inc., HFM-25) at 23 °C and 35% humidity according to the ASTM C518 international standard. The calibration was performed using EPS 1450E as a reference material. All samples were sanded prior the measurement to ensure uniform contact between the sample and the plates. The thermal conductivity measurements were measured and reported after four weeks of storage. Compression tests were performed with a ZwickRoell Materials Testing Machine, Zwicki Z2.5/TN.

Supporting Information

Supporting Information is available from the Wiley Online Library or from the author.

Acknowledgements

The authors acknowledge the support by the Dutch Ministry of Education, Culture and Science (Gravity Program 024.005.020–Interactive Polymer Materials IPM).

Conflict of Interest

Authors declare no conflicts of interest.

Data Availability Statement

The data that support the findings of this study are available from the corresponding author upon reasonable request.

Keywords

aerogels, Mannich polyol, polycarbonate, polyurethane, upcycling

Received: April 28, 2025
Revised: June 21, 2025
Published online: July 11, 2025

[1] A. L. Andrady, M. A. Neal, *Phil. Trans. R. Soc. B* **2009**, *364*, 1977.
[2] R. Geyer, J. R. Jambeck, K. L. Law, *Sci. Adv.* **2017**, *3*, 1700782.
[3] H. Jung, G. Shin, H. Kwak, L. T. Hao, J. Jegal, H. J. Kim, H. Jeon, J. Park, D. X. Oh, *Chemosphere* **2023**, *320*, 138089.
[4] M. Hong, E. Y. X. Chen, *Green Chem.* **2017**, *19*, 3692.
[5] L. T. J. Korley, T. H. Epps 3rd, B. A. Helms, A. J. Ryan, *Science* **2021**, *373*, 66.
[6] C. Pantazidis, C. Wang, Ž. Tomović, *Small* **2024**, *20*, 2403931.
[7] Y. Xiong, C. Wang, L. Dong, Ž. Tomović, *Adv. Funct. Mater.* **2025**, *35*, 2420472.
[8] E. J. Hoekstra, C. Simoneau, *Crit. Rev. Food Sci. Nutr.* **2013**, *53*, 386.
[9] J. T. Bendler, D. G. Legrand, *Handbook of Polycarbonate Science and Technology*, 1st ed., CRC Press, Boca Raton **1999**.
[10] D. Kyriacos, *Polycarbonates, 457, Brydson's Plastics Materials*, 8th ed., Butterworth-Heinemann, Oxford UK **2017**.
[11] J. G. Kim, *Polym. Chem.* **2020**, *11*, 4830.
[12] G. Grause, R. Kärrbrant, T. Kameda, T. Yoshioka, *Ind. Eng. Chem. Res.* **2014**, *53*, 4215.
[13] X. Zhou, M. Chai, G. Xu, R. Yang, H. Sun, Q. Wang, *Green Chem.* **2023**, *25*, 952.
[14] E. Quaranta, D. Sgherza, G. Tartaro, *Green Chem.* **2017**, *19*, 5422.
[15] T. Do, E. R. Baral, J. K. Kim, *Polymer* **2018**, *143*, 106.
[16] K. Saito, F. Eisenreich, T. Türel, Ž. Tomović, *Angew. Chem., Int. Ed.* **2022**, *61*, 202211806.
[17] G. O. Jones, A. Yuen, R. J. Wojtecki, J. L. Hedrick, J. M. Garcia, *Proc. Natl. Acad. Sci. USA* **2016**, *113*, 7722.
[18] K. Saito, P. Schara, F. Eisenreich, Ž. Tomović, *ACS Sustainable Chem. Eng.* **2025**, *13*, 3766.
[19] D. Randall, S. Lee, *The Polyurethanes Book*, 1st ed., Wiley, New York **2003**.
[20] B. Eling, Ž. Tomović, V. Schädler, *Macromol. Chem. Phys.* **2020**, *221*, 2000114.
[21] N. V. Gama, A. Ferreira, A. Barros-Timmons, *Materials* **2018**, *11*, 1841.
[22] L. D. H. Anh, Z. Pásztory, *J. Build. Eng.* **2021**, *44*, 102604.
[23] B. Notario, J. Pinto, E. Solorzano, J. A. de Saja, M. Dumon, M. A. Rodríguez-Pérez, *Polymer* **2015**, *56*, 57.
[24] R. Baetens, B. P. Jelle, A. Gustavsen, *Energy Build.* **2011**, *43*, 761.
[25] M. A. Aegerter, N. Leventis, M. M. Koebel, *Aerogels Handbook*, 1st ed., Springer, New York **2011**.
[26] M. Ionescu, *Chemistry and Technology of Polyols for Polyurethanes*, Rapra Technology Limited, Shawbury UK **2005**.
[27] C. Wang, Y. Guo, T. Türel, Ž. Tomović, *ACS Appl. Mater. Interfaces* **2024**, *16*, 35604.
[28] G. Biesmans, D. Randall, E. Francais, M. Perrut, *J. Non-Cryst. Solids* **1998**, *225*, 36.
[29] B. Merillas, J. Martín-de León, F. Villafañe, M. A. Rodríguez-Pérez, *ACS Appl. Polym. Mater.* **2021**, *3*, 4607.
[30] Z. Zhu, M. B. F. G. Snellings, M. M. Koebel, W. J. Malfait, *ACS Appl. Mater. Interfaces* **2017**, *9*, 18222.
[31] S. Donthula, C. Mandal, T. Leventis, J. Schisler, A. M. Saeed, C. Sotiriou-Leventis, N. Leventis, *Chem. Mater.* **2017**, *29*, 4461.
[32] S. Malakooti, A. B. M. S. ud Doulah, Y. Ren, J. L. Hedrick, J. M. Garcia, S. L. Vivod, C. Sotiriou-Leventis, N. Leventis, H. Lu, *ACS Appl. Polym. Mater.* **2021**, *3*, 5727.
[33] T. Do, E. R. Baral, J. G. Kim, *Polymer* **2018**, *143*, 106.
[34] I. Rotaru, M. Ionescu, D. Donescu, M. Vuluga, V. Purcar, *U.P.B. Sci. Bull. Ser. B* **2007**, *69*, 35.
[35] R. K. Gupta, M. Ionescu, X. Wan, D. Radojcic, Z. S. Petrovic, *J. Polym. Environ.* **2015**, *23*, 261.
[36] T. Gandhi, M. Patel, B. Dholakiya, *J. Polym. Eng.* **2015**, *35*, 533.
[37] Y. Guo, M. Muuronen, F. Lucas, R. P. Sijbesma, Ž. Tomović, *ChemCatChem* **2023**, *15*, 202201362.

[38] A. B. M. Shaheen ud Doulah, C. Mandal, H. M. Far, V. A. Edlabadkar, R. U. Soni, S. Y. Owusu, N. Leventis, C. Sotiriou-Leventis, *ACS Appl. Polym. Mater* **2023**, *5*, 6851.
[39] C. Chidambareswarapattar, P. M. McCarver, H. Luo, H. Lu, C. Sotiriou-Leventis, N. Leventis, *Chem. Mater.* **2013**, *25*, 3205.
[40] W. J. Malfait, H. P. Ebert, S. Brunner, J. Wernery, S. Galmarini, S. Zhao, G. Reichenauer, *J. Sol-Gel Sci. Technol.* **2024**, *109*, 569.
[41] B. Merillas, F. Villafañe, M. A. Rodríguez-Pérez, *Nanomaterials* **2022**, *12*, 2409.
[42] D. Kumar, M. Alam, P. X. W. Zou, J. G. Sanjayan, R. A. Memon, *Renewable and Sustainable Energy Rev.* **2020**, *131*, 110038.